HHS Public Access

Author manuscript

ACS Appl Mater Interfaces. Author manuscript; available in PMC 2023 March 29.

Published in final edited form as:

ACS Appl Mater Interfaces. 2022 June 29; 14(25): 28548–28558. doi:10.1021/acsami.2c04671.

Metal-Organic Coordination Polymer for Delivery of a Subunit Broadly Acting Influenza Vaccine

Meital Eckshtain-Levi[1,*], **Cole J. Batty**[1,*], **Liubov M. Lifshits**[1,*], **Brandon McCammitt**[1], **Kathryn M. Moore**[1], **Eva A. Amouzougan**[1], **Rebeca T. Stiepel**[1], **Eliza Duggan**[2], **Ted M. Ross**[3,4], **Eric M. Bachelder**[1], **Kristy M. Ainslie**[1,5,6,#]

[1]Division of Pharmacoengineering and Molecular Pharmaceutics, Eshelman School of Pharmacy, University of North Carolina at Chapel Hill, Chapel Hill, NC, USA.

[2]North Carolina School of Science and Mathematics, Durham, NC, USA

[3]Center for Vaccines and Immunology, University of Georgia, Athens, GA, USA.

[4]Department of Infectious Diseases, University of Georgia, Athens, GA, USA.

[5]Department of Microbiology and Immunology, School of Medicine, University of North Carolina at Chapel Hill, Chapel Hill, NC, USA.

[6]Joint Department of Biomedical Engineering, University of North Carolina at Chapel Hill and North Carolina State University, USA.

Abstract

A zinc-carnosine (ZnCar) metal-organic coordination polymer was fabricated in biologically relevant HEPES buffer for use as a vaccine platform. *In vitro,* ZnCar exhibited significantly less cytotoxicity than a well-established zeolitic imidazolate framework (ZIF-8). Adsorption of CpG on the ZnCar surface resulted in enhanced innate immune activation compared to soluble CpG. The model antigen ovalbumin (OVA) was encapsulated in ZnCar and exhibited acid-sensitive release *in vitro*. When injected intramuscularly on day 0 and 21 in C57BL/6 mice, OVA-specific serum total IgG and IgG1 were significantly greater in all groups with ZnCar and antigen compared to soluble controls. Th1-skewed IgG2c antibodies were significantly greater in OVA and CpG groups delivered with ZnCar for all time points, regardless of whether the antigen and adjuvant were co-formulated in one material or co-delivered in separate materials. When broadly acting Computationally Optimized Broadly Reactive Antigen (COBRA) P1 influenza hemagglutinin (HA) was ligated to ZnCar via its His-tag, significantly greater antibody levels were observed at all time points compared to soluble antigen and CpG. ZnCar-formulated antigen elicited increased peptide presentation to B3Z T cells *in vitro* and production of IL-2 after *ex vivo* antigen recall of splenocytes isolated from vaccinated mice. Overall, this work displays

[#]**Corresponding Author Address:** Kristy M. Ainslie, Professor and Chair, Division of Pharmacoengineering and Molecular Pharmaceutics, UNC Eshelman School of Pharmacy, 4211 Marsico Hall, 125 Mason Farm Road, Chapel Hill, NC 27599, United States, ainsliek@email.unc.edu.

[*]Authors contributed equally

Supporting information

Synthesis and characterization of materials by SEM and PXRD, drug release profiles, cell viability assays, and full statistical analysis supplied as Supporting Information.

the formation of a zinc-carnosine metal-organic coordination polymer that can be applied as a platform for recombinant protein-based vaccines.

Graphical Abstract:

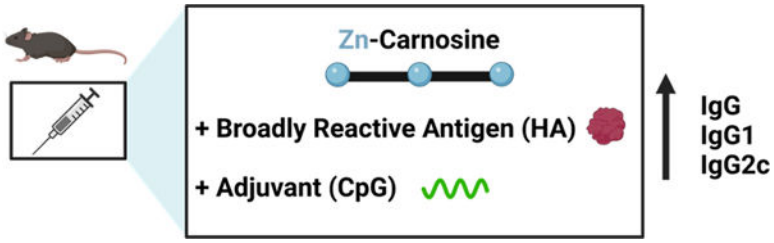

Keywords

zinc; carnosine; coordination polymer; metal-organic framework (MOF); vaccine delivery; universal influenza vaccine; hemagglutinin

INTRODUCTION

Metal-organic coordination polymers are emerging as a promising class of materials for drug and vaccine delivery. Compared to other well-established vaccine delivery platforms, such as viral, polymeric, and lipidic platforms that require intricate and expensive manufacturing procedures, metal-organic coordination polymers can achieve facile and cost-effective synthesis and incorporation of drugs or vaccine antigens. Also, metal ions incorporated within metal-organic materials enable easy functionalization with groups that exhibit high affinity toward metals (like His-tag or phosphate groups, commonly present in biomolecules), which can be difficult to achieve in other platforms. Metal-based functionalization can be utilized to load molecules of interest via surface attachment or encapsulation by creating pre-nucleation clusters via electrostatic interactions. Additionally, synthesis of metal-organic materials under non-denaturing biocompatible conditions offers the possibility of incorporating of proteins without altering their antigenicity. Finally, the ability of metal-organic materials to protect biomolecules from thermal exposure could permit storage at ambient temperature, as opposed to the cold-chain storage conditions required for conventionally used platforms.[1]

Reported as 1-dimensional (1D), 2D and 3D structures, metal-based coordination polymers with organic ligands that form 2D and 3D structures commonly contain internal pores and are referred to as metal-organic frameworks (MOFs) (Figure 1A, 1B). Here we report the use of a coordination polymer comprising the dipeptide carnosine and zinc ions (Zn^{2+}) (ZnCar) for incorporation of antigen and adjuvant as an influenza vaccine delivery system. Carnosine is a naturally occurring peptide in muscle and brain tissue, whose histidine contains an imidazole group, imparting inherent acid sensitivity that will break its coordination with metal ions near a pH of 5.0.[2] This pH switch allows for a triggered release of cargo upon internalization by phagocytic cells (e.g. macrophages, dendritic cells (DCs)) and exposure to the acidic pH of the endo/lysosome.[3] This is ideal for a vaccine

carrier as we have previously shown that acid-sensitivity in a carrier significantly increases vaccine efficacy.[4–6]

A 3D MOF constructed from carnosine and Zn^{2+} (ZnCar-MOF) has been reported previously.[7, 8] However, the fabrication process for this MOF relies on harsh solvents (e.g. dimethylformamide, ethanol) and elevated temperature, which can denature protein antigens and lead to the generation of non-neutralizing antibodies.[9] Generation of metal-organic coordination polymers in more biologically relevant solutions could result in enhanced vaccine efficacy, compared to those in organic solutions; however, different constructs may form in place of 3D MOFs upon changes in synthesis conditions.[10] One such construct is a 1D metal-organic coordination polymer. 1D metal-organic coordination polymers are formed by metal ions interconnected by bridging linkers in an infinite chain-like fashion (Figure 1B), while any remaining coordination sites of the metal ions are capped with ligands that lack extension points, such as most solvent molecules. While 3D MOFs are typically more porous structures than 1D metal-organic coordination polymers, both are capable of serving as drug delivery vehicles via drug attachment to the surface or encapsulation in the void space within the structures.[11–13]

Influenza vaccines are used to prevent pandemics like those observed in 1918, 1957, 1968, and 2009, as well as pandemics predicted to occur in the future.[14] The 2009 H1N1 influenza pandemic strain lead to over a half-million deaths worldwide.[15] Historically, the strains selected for seasonal influenza vaccines can differ from circulating strains because of antigenic shift and/or drift, which can result in significantly reduced vaccine efficacy. Therefore, more broadly reactive or universal approaches are needed to provide enhanced protection over the current vaccines.[16] To identify a broadly reactive influenza antigen that can elicit protective responses against a wider array of circulating influenza viruses, Computationally Optimized Broadly Reactive Antigen (COBRA) was developed. COBRA uses iterative layered consensus building from hemagglutinin (HA) sequences of circulating influenza isolates to construct antigens capable of eliciting a broadly reactive immune response.[17] These antigens could protect against past and future seasonal and novel pandemic influenza strains including pandemic H1N1 subtypes.[17]

A broadly protective and safely applied COBRA HA vaccine has many advantages compared to conventional seasonal flu vaccine formulations; however, recombinant protein antigens tend to activate the immune response only weakly without the addition of an adjuvant. For this reason, we have formulated toll-like receptor 9 (TLR 9) agonist cytosine-phosphate-guanine (CpG) with COBRA H1 HA.[17] CpG is FDA approved as an adjuvant in hepatitis B vaccine Heplisav-B®. Herein, we report the evaluation of a zinc-carnosine metal-organic coordination polymer for delivery of COBRA H1 HA and CpG for application as an influenza vaccine. The platform was characterized by scanning electron microscopy (SEM), high performance liquid chromatography (HPLC), zeta potential, and powder X-ray diffraction (PXRD) spectroscopy, and the generated X-ray diffraction spectra were compared to the previously reported ZnCar-MOF.[7, 8] We evaluated the humoral and cellular response with model antigen ovalbumin (OVA) and COBRA H1 HA in a mouse model. Our research highlights a facile and biocompatible method to apply a metal-organic platform for generation of subunit vaccines.

RESULTS AND DISCUSSION

Zinc acetate and carnosine were stirred overnight in 0.1M HEPES buffer at neutral at 37°C (Figure 1C, 2A). HEPES buffer was chosen for its low binding to zinc ions.[19] The product (ZnCar) was determined by HPLC to be composed of 77.00 ± 2.59 % carnosine by mass, consistent with a 1:1 molar ratio of zinc and carnosine. The PXRD spectrum of ZnCar was compared to a simulated spectrum of ZnCar-MOF reported in literature[7] and to a simulated spectrum of a 1D zinc-carnosine coordination polymer (ZnCar-CP) (Figure 2C), the structure of which was modeled utilizing Expo2014 software.[20] The experimental PXRD pattern of ZnCar (the product generated by our group in HEPES buffer) closely resembled the simulated powder diffraction pattern for a ZnCar-CP but differed from that of the ZnCar-MOF (Figure 2C). SEM revealed that the morphologies of these materials differed as well; while ZnCar-MOF consisted of well-defined rectangular prismatic microcrystals (Supplementary Figure S1), ZnCar formed thin nanofibers (Figure 2A). Moreover, cryogenic electron microscopy (cryo-EM) of ZnCar revealed lattice fringes indicative of stacks of polymeric chains on a nanoscale level (Figure 2B). Whereas ZnCar-MOF is a 3D MOF, ZnCar-CP (molecular model) consists of Zn cations and carnosine ligands linked in an infinite 1D polymeric chain. Solvent molecules (like water) were not modeled and are expected to occupy remaining coordination sites of Zn cations in ZnCar-CP structure. Furthermore, the bulk material of ZnCar-CP is composed of numerous polymeric chains stacking next to each other, allowing for solvent or drug entrapment between neighboring chains.

ZnCar-CP and ZnCar-MOF are closely related structures, and either could be formed depending on slight variations in the synthesis conditions. For example, when synthesis was performed in a mixture of HEPES buffer and ethanol, PXRD spectrum of the obtained material matched the spectrum of ZnCar-MOF, while synthesis in HEPES buffer alone resulted in the formation of ZnCar (Supplementary Figure S2), which we hypothesize has ZnCar-CP structure. Additionally, when the ZnCar-MOF synthesis procedure[7] was followed and the reaction mixture was stirred, ZnCar-MOF was obtained (Supplementary Figure S1); however, when the same procedure was followed without stirring the reaction mixture, the PXRD of the obtained material matched the PXRD of ZnCar and not of ZnCar-MOF (Supplementary Figures S3, S4), and the morphology of the obtained material resembled ZnCar (Supplementary Figure S4B).

Further biophysical characterization of ZnCar was performed. The surface charge of ZnCar was evaluated after 3 h incubation in HEPES and PBS buffers at neutral pH. The zeta potential of the ZnCar incubated in HEPES was near neutrality (1.56 ± 2.35 mV), whereas ZnCar incubated in PBS had a significantly more negative surface charge (−21.91 ± 3.40 mV). This was likely due to phosphate adsorption to the ZnCar surface (caused by high affinity of phosphate groups for Zn cations[21]), as illustrated by apparent crystal growth on the material surface (Supplementary Figure S5B). The scalability of ZnCar synthesis was also investigated. Synthesis was performed at a 900 mL scale (60X scale up) in otherwise identical conditions (in 0.1M HEPES at neutral pH with overnight stirring at 37°C). The resulting ZnCar had similar morphology and crystallinity as ZnCar synthesized at a smaller scale (Supplementary Figure S6). In addition, upon scale up, the reaction yield

was increased from ~50% to ~100% yield. This observed increase in yield may be attributed to the volume of glassware used and the glass surface acting as a nucleation site for the formation of the polymer (Supplementary Table S1).

In vitro cytocompatibility of ZnCar was evaluated with 3T3 fibroblasts and DC2.4 dendritic cells (DCs). Cell viability following treatment with ZnCar or ZIF-8, a well-established zeolitic imidazolate framework (ZIF), was determined. ZIFs are one of the most extensively explored metal-organic materials and ZIF-8 has been previously applied as a drug delivery vehicle for cancer and infectious disease vaccines.[1, 22–24] Our results indicate that in both fibroblasts and DCs, ZnCar was significantly less toxic than ZIF-8 at both 24 and 48 hours. The reduced cytotoxicity compared to ZIF-8 was especially pronounced in DCs relative to non-phagocytic fibroblasts (Figure 3; Supplementary Figure S7; Table 1). The cytotoxicity in DCs is important, as DCs are professional antigen presenting cells and therefore vital in coordinating vaccine responses to protein antigens.[16] The IC_{50} of each of the reagents used to form ZnCar and ZIF-8 was determined in fibroblasts, and was much lower for the zinc salts relative to the ligands, indicating that the cytotoxicity of these materials was primarily driven by zinc (Supplementary Figure S8). Based on this and the decreased observed cytotoxicity in comparison to ZIF-8, it is likely ZnCar will have the same or decreased *in vivo* toxicity compared to ZIF-8, a platform that has demonstrated minimal toxicity *in vivo*.[1, 25, 26]

To assess ZnCar as a vaccine platform, we formulated a protein antigen and CpG adjuvant with ZnCar. To incorporate adjuvant, CpG was electrostatically adsorbed on the surface of the material (ZnCar-CpG; the "-" symbol represents surface association, in this case CpG to the ZnCar surface) (Figure 4A). The final loading quantified for CpG on the ZnCar-CpG composite was 52.9 Mg/mg of material. The addition of negatively charged CpG to ZnCar resulted in a net negative surface charge of −6.18 ± 1.63 mV, compared to the vehicle charge of ZnCar (1.56 ± 2.35 mV) (Figure 4B). To evaluate the *in vitro* innate immune activation of ZnCar and ZnCar-CpG, the materials were incubated with macrophages and compared to equal concentrations of soluble CpG. ZnCar-CpG was not significantly more cytotoxic than empty ZnCar after 24 hours (Figure 4C); however, generation of innate signaling mediator nitric oxide was significantly greater in macrophages cultured with ZnCar-CpG compared to soluble CpG or ZnCar alone (Figure 4D). Treatment of macrophages with ZnCar-CpG also induced significantly greater secretion of inflammatory cytokines interleukin 6 (IL-6) and tumor necrosis factor alpha (TNF-α) after 24 hours compared to soluble CpG or ZnCar alone (Figures 4E, 4F). This indicates a potential for CpG adsorbed to ZnCar material to stimulate an innate immune response and the potential for dose sparing of adjuvant when delivered as a ZnCar-CpG composite.

To encapsulate the model antigen OVA within the coordination polymer, OVA was added to the reaction solution during the formation of ZnCar (OVA/ZnCar; symbol "/" represents encapsulation, in this case OVA encapsulated in ZnCar) (Figure 5A). Loading of OVA in OVA/ZnCar composite was observed to be 4.3 μg/mg of material. The release of OVA from OVA/ZnCar at neutral pH illustrated a burst of approximately 18%, likely due to surface adsorption of protein, and is released only incrementally for an additional 24 hours (Supplementary Figure S9A). Further, the release was shown to be acid-sensitive, with

approximately 20% released after 24 hours in pH 7.4 HEPES buffer, but nearly 100% released in pH 5.0 buffer (Figure 5B).

The toxicity and efficacy of antigen presentation from DCs to T cells was evaluated *in vitro* using the B3Z T cell clone (Figure 5C-D). Our results indicate that ZnCar encapsulating OVA with or without CpG (OVA/ZnCar-CpG and OVA/ZnCar) significantly enhanced antigen cross-presentation relative to the soluble antigen. This could be a function of particle delivery of the antigen[27] as well as the acid-sensitivity of the complex.[4]

To evaluate the humoral response to OVA and CpG formulated with ZnCar, OVA was encapsulated in ZnCar (OVA/ZnCar), and CpG was either co-formulated on the same composite (OVA/ZnCar-CpG) or delivered simultaneously in separately generated materials (OVA/ZnCar + ZnCar-CpG). Our group and others have shown that delivery of protein antigen and adjuvant in separate particles can invoke increased vaccine responses[9, 28, 29] in comparison to antigen and adjuvant in the same particle. These ZnCar formulations were administered to C57BL/6 mice on days 0 and 21 by intramuscular (IM) injection, and the humoral response was evaluated. Serum IgG (Figure 5E; Supplementary Table S2), IgG2c (Figure 5F; Supplementary Table S3), and IgG1 (Figure 5G; Supplementary Table S4) titers were measured at days 14, 28, and 42. An IM route was chosen because it is the most clinically relevant route and our previous studies have shown it results in efficient stimulation of the antigen presenting cells.[30] The use of ZnCar as a delivery vehicle facilitated greater total IgG and IgG1 antibody production by day 42 compared to soluble OVA and soluble CpG (solOVA + solCpG). However, the presence of CpG was required to generate Th1 skewed IgG2c response, with the OVA/ZnCar-CpG and OVA/ZnCar + ZnCar-CpG treated mice generating significantly greater antibody titers at all time points compared to all other groups. Although many current vaccines are formulated with the Th2 skewing adjuvant alum (e.g. Biothrax, DTaP, MenB, Gardasil), Th1 responses are needed for protection against intracellular pathogens like viruses, some bacteria, fungi and parasites,[31] and therefore a Th1 response is needed for many vaccines. Overall, these results illustrate that OVA-loaded ZnCar with and without CpG can generate significant antigen-specific humoral responses. Previous studies with OVA and CpG-loaded ZIF-8 MOF also illustrate significantly higher total IgG titers over soluble OVA and CpG,[32, 33] however, our data indicates that ZnCar material has reduced cytotoxicity compared to ZIF-8 MOF (Figure 3), which could help to limit vaccine side effects.

Next, we assessed ZnCar for use as a broadly acting influenza vaccine with COBRA H1 HA (HA). His-tagged HA was employed, as this tag allowed complexation with Zn ions on the surface of ZnCar. HA loading was determined to be much higher than that of OVA (which lacks His-tag) at 45.6 Mg HA/mg of material. The release of HA from ZnCar-HA at neutral pH demonstrated gradual and time-dependent release (Supplementary Figure S9B). As with OVA/ZnCar, release from ZnCar-HA was acid-sensitive with rapid and complete release of HA in pH 5.0 buffer (Supplementary Figure S9C). When ZnCar-HA (Figure 6A) was used to vaccinate C57BL/6 mice in a prime-boost schedule, the group with HA and CpG (co-administered in separate vehicles) had significantly greater antibody production than control groups (Figures 6C-E, Supplementary Table S5-7).

To evaluate the cellular response *ex vivo*, splenocytes were isolated from HA-vaccinated mice and cultured in the presence of HA. In the supernatant of these restimulated splenocytes, no significant difference in interferon gamma (IFN-γ) secretion was observed, but IL-2 secretion was significantly greater in the ZnCar-delivered group compared to a group receiving soluble antigen and adjuvant, indicating a greater degree of antigen-specific T cell responses (Figure 6B). These findings support previous studies which indicate that vaccination with ZIF-8 MOFs associated with OVA and CpG lead to increased proliferation of T cells[33] as well as increased levels of pro-inflammatory cytokines upon antigen restimulation.[32]

Based on the obtained results, ZnCar demonstrated promise as a vaccine platform. It permitted drug loading *via* both encapsulation and surface attachment. ZnCar retains the advantages of other coordination polymer materials, such as facile and inexpensive synthesis, while further improving the biocompatibility of the material. Carnosine is naturally present in the human body in muscle and brain tissue, contrasting with the exogenous 2-methylimidazole ligand utilized in ZIF-8. Combined with its rapid degradability in acidic conditions, this provides a promising safety profile for clinical translation. Herein we have demonstrated ZnCar's potent performance as a vaccine platform *in vitro* and *in vivo*. Future work will be focused on further elucidation of the mechanism of this enhanced performance, its capacity to generate a long-lasting protective immune-response, and the application of this platform to delivery of other therapeutics.

CONCLUSION

In conclusion, we introduced a facile and biocompatible synthesis of a metal-organic coordination material comprised of zinc and carnosine. Complementary methods such as cryo-EM and molecular modeling suggest that our ZnCar material is a 1D coordination polymer rather than the 3D ZnCar-MOF previously reported in literature.[7] Infinite coordination polymers are known to exhibit rapid stimulus-dependent depolymerization, a property which may make them more desirable than MOFs for stimulus-dependent drug release applications.[34] ZnCar consists of micron-length fibers that can encapsulate protein antigens as well as associate protein antigens and CpG to their surface. ZnCar exhibited reduced cytotoxicity compared to ZIF-8 MOF *in vitro*. A dose-sparing response was observed for CpG wherein less CpG was needed to stimulate innate immune activity in the form of ZnCar-CpG than soluble CpG *in vitro*. When ZnCar was evaluated *in vivo* as a vaccine platform, whether formulated with OVA or COBRA H1 HA with CpG, a significantly greater Th1 humoral response was observed. Moreover, cytokine generation with antigen recall indicates an antigen-specific cellular response. These results illustrate the potency of ZnCar metal-organic coordination polymer in inducing antigen-specific humoral and cellular responses when formulated with recombinant protein antigens. This is promising for future applications working towards achieving an effective immune response from broadly acting influenza vaccines.

MATERIALS AND METHODS

All chemicals were purchased from Sigma (St. Louis, MO) and used as purchased, unless otherwise indicated. Assays, biologics, and disposables were purchased from Thermo Fisher Scientific (Waltham, MA) unless otherwise indicated.

Synthesis of Metal Organic Carriers

For ZnCar, 0.1M HEPES solution was prepared by diluting an aliquot of sterile 1M HEPES buffer solution of pH 7.4 (Corning, Corning, NY) in molecular biology grade water (Corning) and adjusting the pH of the resulting solution to 7.4 with 1M aqueous NaOH solution. Carnosine (51.3 mg, 0.227 mmol) was dissolved in 5 ml of HEPES solution. Zinc acetate dihydrate (50 mg, 0.227 mmol) was dissolved in 10 ml of HEPES solution. Carnosine and zinc acetate solutions were mixed together, and the reaction mixture was stirred at 37ºC for 18 h. The reaction mixture was cooled to room temperature and the resulting precipitate was isolated by centrifugation (22,000 x g, 20 min, 4ºC). The pellet was washed with Milli-Q water (twice), re-suspended in 5 mL of Milli-Q water, frozen at −80ºC and lyophilized to produce ZnCar as a white powder (52 mg, 51% yield).

OVA/ZnCar was synthesized by mixing carnosine (51.3 mg, 0.227 mmol), zinc acetate dihydrate (50 mg, 0.227 mmol), and ovalbumin (OVA) (4 mg, 0.000093 mmol; Invivogen Endofit OVA, San Diego, CA) in 15 ml of HEPES buffer (0.1M, pH = 7.4). The reaction mixture was stirred at 37ºC for 18 h. The reaction mixture was cooled down to room temperature and the resulting precipitate was isolated by centrifugation (22,000 x g, 20 min, 4ºC). Supernatant containing unencapsulated OVA was removed, and the pellet was washed with Milli-Q water (twice), re-suspended in 5 mL of Milli-Q water, frozen at −80ºC for and lyophilized to produce OVA/ZnCar as a white powder. To characterize OVA loading in OVA/ZnCar material, samples were decomposed in acetate buffer (pH = 5.0) at 1 mg/mL concentration, carnosine removed by desalting with a 3 kDa Amicon Ultra-0.5 centrifugal filter, and the retentate analyzed with a BCA assay. OVA loading was determined to be 4.28 μg/mg.

CpG ODN 1826 (CpG) (Invivogen) was adsorbed on ZnCar by mixing a suspension of ZnCar in HEPES buffer (0.1M, pH = 7.4) and an aliquot of CpG stock solution in sterile water (40μM), resulting in the formation of ZnCar-CpG material. Loading of CpG in ZnCar-CpG was confirmed by measuring the absorbance of the supernatant (260 nm) after centrifugation (22,000 x g, 20 min, 4ºC). Loading and encapsulation efficiency were determined to be 52.9 μg/mg and 100%, respectively. OVA/ZnCar-CpG material was synthesized in the identical way, with OVA/ZnCar used in place of empty ZnCar. COBRA P1 HA (referred to as HA; containing a His-tag) was used and generated as previously indicated.[35–38] HA was loaded onto ZnCar by mixing a suspension of ZnCar in HEPES buffer (0.1M, pH = 7.4) and an aliquot of HA in HEPES buffer, resulting in formation of ZnCar-HA. HA loading on ZnCar-HA was evaluated with a BCA assay and determined to be 45.6 μg/mg. Empty ZnCar and loaded ZnCar materials exhibited the same morphology by SEM (Supplementary Figure S9).

ZnCar-MOF[7] and ZIF-8 MOF[39] were synthesized as previously indicated.

Characterization

ZnCar Structure Determination—Numerous attempts to obtain a crystal of ZnCar material suitable for crystal structure determination were performed but none of the methods produced a crystal of suitable quality. Regular synthesis conditions (HEPES buffer pH = 7.4, 37ºC, 18 h, stirring) produced nanofibrous material (Supplementary Figure S10A) not suitable for single X-ray diffraction (SXRD) analysis due to the small crystal dimensions. Performing the synthesis without stirring (HEPES buffer pH = 7.4, 37ºC, 18 h, no stirring) did not improve crystallinity of the product. When crystals were grown at room temperature with no stirring, spherical aggregates composed of microcrystals were obtained (Supplementary Figure S11); similar results were obtained when crystals were grown at 4ºC with no stirring. When these polycrystalline spheres were cut in half with a razor, SEM demonstrated that the spheres' interiors consisted of fibers very similar to the fibers synthesized at 37ºC (Supplementary Figure S12). The experimental PXRD of ZnCar synthesized at room temperature fully matched the experimental PXRD of ZnCar synthesized at 37ºC (Supplementary Figure S13), indicating that it is the same compound. Unfortunately, the spherical aggregates obtained by room temperature synthesis (25–50 μm) were not suitable for SXRD due to their polycrystallinity, and the microcrystals (1 μm or less) composing those spheres were not suitable for SXRD due to their small size and their intergrowth.

When the synthesis conditions were altered to include ethanol (HEPES buffer pH = 7.4, ethanol, no stirring; aqueous:ethanol at 2:1 ratio), SXRD-suitable crystalline material was formed. When this crystalline material was analyzed with SXRD, it revealed the crystal structure of the 3D ZnCar-MOF reported in literature.[7] The PXRD spectrum simulated from this crystal structure fully matched the simulated PXRD spectrum of ZnCar-MOF but differed from the experimental PXRD of ZnCar synthesized in HEPES buffer alone (Supplementary Figure S2), indicating that those two materials are not the same. So, while addition of an organic solvent like ethanol improved the crystallinity of the material, it resulted in the formation of a different structure; meanwhile, the material formed in the absence of ethanol was not suitable for SXRD. Next, we attempted structure determination using microcrystal electron diffraction (microED). However, even with cryogenic sample preparation, diffraction from the ZnCar material was too weak to elucidate the structure.

Due to the lack of SXRD-suitable or micro-ED-suitable material, molecular modeling was utilized. A molecular model of the ZnCar structure was based on the experimental PXRD spectrum of ZnCar (HEPES buffer pH = 7.4, 37ºC, 18 h, stirring) and was generated via Expo2014 software.[20] The crystal structure of ZnCar-MOF (CCDC 949242) was used as a starting point for the modeling.

Endotoxin, Imaging, and Zeta Potential—Endotoxin was evaluated using the Pierce LAL chromogenic endotoxin quantitation kit in accordance with the manufacturer instructions. All samples had undetectable levels of endotoxin (<0.1 EU/mg). SEM (Hitachi S-4700 with EDS, Tokyo, Japan) and PXRD (Rigaku SmartLab diffractometer, Tokyo, Japan) were carried out at UNC CHANL. For Cryo-EM imaging, ZnCar samples were suspended at 1 mg/mL in molecular grade water immediately prior to application to plasma-

cleaned R1.2/1.3 Quantifoil Cu grids. Samples were blotted and frozen using a Vitrobot Mark IV. Data was collected at the UNC at Chapel Hill CryoEM Core Facility with a 200 keV Thermo Fisher Scientific Talos Arctica G3 equipped with a Gatan K3 direct electron detector. Zeta potential was determined on a NanoBrook 90Plus Zeta Particle Size Analyzer (Holtsville, NY).

HPLC Analysis of Carnosine Content—To quantify ZnCar carnosine content, ZnCar was dissolved in a 0.1% trifluoroacetic acid (TFA). Carnosine loading was quantified by high performance liquid chromatography (HPLC, Agilent 1100 series, Santa Clara, CA) using a 0.1% TFA in water/0.1% TFA in acetonitrile gradient method through an Aquasil C18 column (150 mm length, 4.6 mm inner diameter, 5 μm pore size) with a C8 guard column cartridge and a UV detection wavelength of 220 nm. Theoretical mass loading of carnosine at a 1:1 molar ratio was determined to be 77.37%.

In vitro Experiments: All cell lines (RAW 264.7 murine macrophages, DC2.4 dendritic cells, and 3T3 fibroblasts; ATCC, Manassas, VA) and maintained according to ATCC guidelines. For viability experiments, cells were plated overnight at 5×10^4 cells/well in 100 μL of their respective media. Particle suspensions or soluble controls in 100 μL of their respective media were added to cells for the indicated time points. Media was removed and cell viability was determined with an MTT (Sigma M2128) assay as previously described.[40]

B3Z T cells were obtained from Dr. Nilabh Shastri (Johns Hopkins) and maintained and used as previously outlined.[4] Briefly, DC2.4 cells were seeded overnight at 5×10^4 cells/well in 100 μL RPMI 1640 containing L-glutamine and HEPES (Corning 10–041-CV), with 10% fetal bovine serum (Avantor 97068–085), 1% penicillin/streptomycin (Gibco 15140–122), MEM non-essential amino acids (Gibco 11140050), and 50 μM beta mercaptoethanol (Sigma) overnight. Media was removed and cells were treated for 24 hours with OVA-containing treatments in 100 μL of the same media and 1×10^5 B3Z cells in the same media but containing 1 mM sodium pyruvate (Gibco 11360070) instead of nonessential amino acids. Media was removed and replaced with 100 μL of a solution containing 0.155 mM chlorophenol red β-d-galactopyranoside (Sigma 59767), 0.125% Nonidet P-40 Substitute (Sigma 74385), and 9 mM MgCl2 (Sigma) in PBS. The plates were developed at room temperature away from light. Plates were centrifuged at 500 x g for 5 minutes and 75 μL of the supernatant was transferred to a new plate and absorbance measured at 570 nm.

For Nitric Oxide experiments, macrophages and fibroblasts were plated in a 96-well plate at a density of 5×10^4 cells/well, incubated at 37°C and left overnight to adhere. The cells were treated with complete medium, soluble CpG, ZnCar and ZnCar-CpG particles for 24 h. The isolated macrophage supernatants were collected and analyzed for nitrite concentration using the Griess reagent (Promega, Madison, WI) and IL-6 and TNF-α concentration using mouse TNF-α and IL-6 Ready-SET-Go sandwich ELISA kits (Fisher).

Antibody Titer and Antigen Recall—Mice (C57Bl/6) were purchased from The Jackson Laboratory (Bar Harbor, ME). All animal experiments were performed in accordance with UNC Institutional Animal Care and Use Committee (IACUC) approval. For experiments, mice received 10 μg of protein (OVA or COBRA HA) and 10 μg of CpG per

mouse per dose. These doses of protein and CpG were selected based on what is commonly reported in literature[41–49] and used in our group[5, 28, 50, 51]. Mice were vaccinated on day 0 and 21, and submandibular blood samples were taken on days 14, 28, and 42. On day 42, mice were sacrificed, and their spleens removed and processed for antigen recall.[28]

Flat-bottomed high-binding polystyrene plates (Corning 29442–322) were coated overnight at 4°C with 1 μg/mL COBRA P1 HA in PBS. Plates were washed three times with 200 μL 0.05% Tween 20 in PBS (PBST), then blocked for two hours at room temperature with 200 μL blocking buffer (3% nonfat instant milk in PBS). Plates were washed three times again. Serum samples were diluted in 100 μL blocking buffer and added to the blocked plates for one hour. Plates were washed three times again. The appropriate secondary antibodies (Goat Anti-Mouse IgG Fc-HRP 1033–05, Goat Anti-Mouse IgG2c-HRP 1078–05, or Goat Anti-Mouse IgG1-HRP 1071–05, Southern Biotech) were diluted in blocking buffer to the highest dilution recommended by the manufacturer, and 100 μL of the resulting secondary antibody solution was added to each well for two hours at room temperature. Plates were washed five times with PBST and developed with 100 μL tetramethylbenzidine (TMB) one component substrate (Southern Biotech 0410–01) before quenching with 50 μL 2 N sulfuric acid. Development times were based on day 42 sera and sera from each day were developed for the same amount of time per each secondary antibody to allow comparison of titers between days. Plates were read for absorbance at 450 nm and corrected for background by subtracting absorbance at 570 nm. Antibody titers were determined by fitting a curve to the background-corrected absorbance vs. dilution using the “log(inhibitor) vs. response -- Variable slope (four parameters)” model in Graphpad Prism 8, then interpolating the dilution value at which the curve intercepts the endpoint value as defined by Frey et al. using a 99.9% confidence level and twelve background controls.[52]

Supplementary Material

Refer to Web version on PubMed Central for supplementary material.

Acknowledgements

Abstract Figure and Figure 1 were created with BioRender.com. This work was performed in part at the Chapel Hill Analytical and Nanofabrication Laboratory, CHANL, a member of the North Carolina Research Triangle Nanotechnology Network, RTNN, which is supported by the National Science Foundation, Grant ECCS-2025064, as part of the National Nanotechnology Coordinated Infrastructure, NNCI. We thank Dr. Chun-Hsing (Josh) Chen and Dr. Amar S. Kumbhar of CHANL for their assistance with PXRD and SEM characterization, respectively. This work was performed in part at the Cryo Electron Microscopy (CryoEM) Core at UNC Chapel Hill, affiliated with the UNC Center for Structural Biology of UNC School of Medicine. UNC Center for Structural Biology is supported by the National Cancer Institute of the National Institutes of Health under award number P30CA016086. The content is solely the responsibility of the authors and does not necessarily represent the official views of the National Institutes of Health. We acknowledge Jared Peck and Dr. Joshua Strauss of the UNC CryoEM Core Facility for technical assistance in this project. We thank Dr. Corrado Cuocci (Istituto di Cristallografia – CNR, Bari, Italy) for insightful discussions regarding the EXPO-2014 modeling software. Funding for this work was supported by NIH NIAID Collaborative Influenza Vaccine Innovation Centers (CIVICs) Contract #75N93019C00052 (PI: Ross) and NIH R01AI147497 (PI: Ainslie). K.M. Moore was supported by NSFGRFP (DGE-1650116) and R.T. Stiepel by National Academies of Science Engineering and Medicine (NASEM) Ford Foundation Pre-Doctoral Fellowship.

References

1. Luzuriaga MA; Welch RP; Dharmarwardana M; Benjamin CE; Li S; Shahrivarkevishahi A; Popal S; Tuong LH; Creswell CT; Gassensmith JJ, Enhanced Stability and Controlled Delivery of Mof-Encapsulated Vaccines and Their Immunogenic Response in Vivo. ACS Appl Mater Interfaces 2019, 11 (10), 9740–9746. [PubMed: 30776885]
2. Rötzschke O; Lau JM; Hofstätter M; Falk K; Strominger JL, A Ph-Sensitive Histidine Residue as Control Element for Ligand Release from Hla-Dr Molecules. Proceedings of the National Academy of Sciences 2002, 99 (26), 16946.
3. Foote JR; Patel AA; Yona S; Segal AW, Variations in the Phagosomal Environment of Human Neutrophils and Mononuclear Phagocyte Subsets. Frontiers in Immunology 2019, 10 (188), 1–11. [PubMed: 30723466]
4. Broaders KE; Cohen JA; Beaudette TT; Bachelder EM; Frechet JM, Acetalated Dextran Is a Chemically and Biologically Tunable Material for Particulate Immunotherapy. Proc Natl Acad Sci U S A 2009, 106 (14), 5497–502. [PubMed: 19321415]
5. Junkins RD; Gallovic MD; Johnson BM; Collier MA; Watkins-Schulz R; Cheng N; David CN; McGee CE; Sempowski GD; Shterev I; McKinnon K; Bachelder EM; Ainslie KM; Ting JP, A Robust Microparticle Platform for a Sting-Targeted Adjuvant That Enhances Both Humoral and Cellular Immunity During Vaccination. J Control Release 2018, 270, 1–13. [PubMed: 29170142]
6. Bachelder EM; Beaudette TT; Broaders KE; Paramonov SE; Dashe J; Frechet JM, Acid-Degradable Polyurethane Particles for Protein-Based Vaccines: Biological Evaluation and in Vitro Analysis of Particle Degradation Products. Mol Pharm 2008, 5 (5), 876–84. [PubMed: 18710254]
7. Katsoulidis AP; Park KS; Antypov D; Martí-Gastaldo C; Miller GJ; Warren JE; Robertson CM; Blanc F; Darling GR; Berry NG, Guest‐Adaptable and Water‐Stable Peptide‐Based Porous Materials by Imidazolate Side Chain Control. Angewandte Chemie 2014, 126 (1), 197–202.
8. Pullin TM Biomolecule Encapsulation in Biocompatible Metal-Organic Frameworks University of Adelaide, 2019.
9. Gallovic MD; Schully KL; Bell MG; Elberson MA; Palmer JR; Darko CA; Bachelder EM; Wyslouzil BE; Keane-Myers AM; Ainslie KM, Acetalated Dextran Microparticulate Vaccine Formulated Via Coaxial Electrospray Preserves Toxin Neutralization and Enhances Murine Survival Following Inhalational Bacillus Anthracis Exposure. Adv Healthc Mater 2016, 5 (20), 2617–2627. [PubMed: 27594343]
10. Biradha K; Ramanan A; Vittal JJJCG, Coordination Polymers Versus Metal− Organic Frameworks. Crystal Growth Design 2009, 9 (7), 2969–2970.
11. Lawson HD; Walton SP; Chan C, Metal–Organic Frameworks for Drug Delivery: A Design Perspective. ACS applied materials interfaces 2021, 13 (6), 7004–7020. [PubMed: 33554591]
12. Zhao H; Xu J; Li Y; Guan X; Han X; Xu Y; Zhou H; Peng R; Wang J; Liu Z, Nanoscale Coordination Polymer Based Nanovaccine for Tumor Immunotherapy. ACS Nano 2019, 13 (11), 13127–13135. [PubMed: 31710460]
13. Suárez-García S; Solórzano R; Alibés R; Busqué F; Novio F; Ruiz-Molina D, Antitumour Activity of Coordination Polymer Nanoparticles. Coordination Chemistry Reviews 2021, 441, 213977.
14. Kilbourne ED, Influenza Pandemics of the 20th Century. Emerg Infect Dis 2006, 12 (1), 9–14. [PubMed: 16494710]
15. CDC, 2009 H1n1 Pandemic (H1n1pdm09 Virus) Centers for Disease Control and Prevention, N. C. f. I. a. R. D. N., Ed. cdc.gov, 2019.
16. Janeway C; Travers P; Walport M; Shlomchik M, Immunobiology 5 ed.; Garland Science: New York, 2001.
17. Carter DM; Darby CA; Lefoley BC; Crevar CJ; Alefantis T; Oomen R; Anderson SF; Strugnell T; Cortes-Garcia G; Vogel TU; Parrington M; Kleanthous H; Ross TM, Design and Characterization of a Computationally Optimized Broadly Reactive Hemagglutinin Vaccine for H1n1 Influenza Viruses. J Virol 2016, 90 (9), 4720–34. [PubMed: 26912624]
18. Patterson A, The Scherrer Formula for X-Ray Particle Size Determination. Physical review 1939, 56 (10), 978.

19. Krężel A; Maret W, The Biological Inorganic Chemistry of Zinc Ions. Archives of Biochemistry and Biophysics 2016, 611, 3–19. [PubMed: 27117234]
20. Altomare A; Cuocci C; Giacovazzo C; Moliterni A; Rizzi R; Corriero N; Falcicchio A, Expo2013: A Kit of Tools for Phasing Crystal Structures from Powder Data. Journal of Applied Crystallography 2013, 46 (4), 1231–1235.
21. Velásquez-Hernández M. d. J.; Ricco R; Carraro F; Limpoco FT; Linares-Moreau M; Leitner E; Wiltsche H; Rattenberger J; Schröttner H; Frühwirt P, Degradation of Zif-8 in Phosphate Buffered Saline Media. CrystEngComm 2019, 21 (31), 4538–4544.
22. Zhang G; Fu X; Sun H; Zhang P; Zhai S; Hao J; Cui J; Hu M, Poly(Ethylene Glycol)-Mediated Assembly of Vaccine Particles to Improve Stability and Immunogenicity. ACS Appl Mater Interfaces 2021, 13 (12), 13978–13989. [PubMed: 33749241]
23. Zhang H; Zhang J; Li Q; Song A; Tian H; Wang J; Li Z; Luan Y, Site-Specific Mof-Based Immunotherapeutic Nanoplatforms Via Synergistic Tumor Cells-Targeted Treatment and Dendritic Cells-Targeted Immunomodulation. Biomaterials 2020, 245, 119983. [PubMed: 32229333]
24. Zhong X; Zhang Y; Tan L; Zheng T; Hou Y; Hong X; Du G; Chen X; Zhang Y; Sun X, An Aluminum Adjuvant-Integrated Nano-Mof as Antigen Delivery System to Induce Strong Humoral and Cellular Immune Responses. J Control Release 2019, 300, 81–92. [PubMed: 30826373]
25. Li S; Wang K; Shi Y; Cui Y; Chen B; He B; Dai W; Zhang H; Wang X; Zhong C; Wu H; Yang Q; Zhang Q, Novel Biological Functions of Zif-Np as a Delivery Vehicle: High Pulmonary Accumulation, Favorable Biocompatibility, and Improved Therapeutic Outcome. Advanced Functional Materials 2016, 26 (16), 2715–2727.
26. Luzuriaga MA; Herbert FC; Brohlin OR; Gadhvi J; Howlett T; Shahrivarkevishahi A; Wijesundara YH; Venkitapathi S; Veera K; Ehrman R; Benjamin CE; Popal S; Burton MD; Ingersoll MA; De Nisco NJ; Gassensmith JJ, Metal-Organic Framework Encapsulated Whole-Cell Vaccines Enhance Humoral Immunity against Bacterial Infection. ACS Nano 2021.
27. Kovacsovics-Bankowski M; Clark K; Benacerraf B; Rock KL, Efficient Major Histocompatibility Complex Class I Presentation of Exogenous Antigen Upon Phagocytosis by Macrophages. Proc Natl Acad Sci U S A 1993, 90 (11), 4942–6. [PubMed: 8506338]
28. Chen N; Gallovic MD; Tiet P; Ting JP; Ainslie KM; Bachelder EM, Investigation of Tunable Acetalated Dextran Microparticle Platform to Optimize M2e-Based Influenza Vaccine Efficacy. J Control Release 2018, 289, 114–124. [PubMed: 30261204]
29. Genito CJ; Batty CJ; Bachelder EM; Ainslie KM, Considerations for Size, Surface Charge, Polymer Degradation, Co-Delivery, and Manufacturability in the Development of Polymeric Particle Vaccines for Infectious Diseases. Adv Nanobiomed Res 2021, 2000041. [PubMed: 33681864]
30. Watkins-Schulz R; Tiet P; Gallovic MD; Junkins RD; Batty C; Bachelder EM; Ainslie KM; Ting JPY, A Microparticle Platform for Sting-Targeted Immunotherapy Enhances Natural Killer Cell- and Cd8(+) T Cell-Mediated Anti-Tumor Immunity. Biomaterials 2019, 205, 94–105. [PubMed: 30909112]
31. Rosenthal KS; Zimmerman DH, Vaccines: All Things Considered. Clin Vaccine Immunol 2006, 13 (8), 821–9. [PubMed: 16893980]
32. Yang Y; Chen Q; Wu J-P; Kirk TB; Xu J; Liu Z; Xue W, Reduction-Responsive Codelivery System Based on a Metal–Organic Framework for Eliciting Potent Cellular Immune Response. ACS Applied Materials & Interfaces 2018, 10 (15), 12463–12473. [PubMed: 29595246]
33. Zhang Y; Wang F; Ju E; Liu Z; Chen Z; Ren J; Qu X, Metal-Organic-Framework-Based Vaccine Platforms for Enhanced Systemic Immune and Memory Response. Advanced Functional Materials 2016, 26 (35), 6454–6461.
34. Spokoyny AM; Kim D; Sumrein A; Mirkin CA, Infinite Coordination Polymer Nano-and Microparticle Structures. Chemical Society Reviews 2009, 38 (5), 1218–1227. [PubMed: 19384433]
35. Carter DM; Darby CA; Lefoley BC; Crevar CJ; Alefantis T; Oomen R; Anderson SF; Strugnell T; Cortés-Garcia G; Vogel TU; Parrington M; Kleanthous H; Ross TM, Design and Characterization of a Computationally Optimized Broadly Reactive Hemagglutinin Vaccine for H1n1 Influenza Viruses. J Virol 2016, 90 (9), 4720–4734. [PubMed: 26912624]

36. Allen JD; Ray S; Ross TM, Split Inactivated Cobra Vaccine Elicits Protective Antibodies against H1n1 and H3n2 Influenza Viruses. PLoS One 2018, 13 (9), e0204284. [PubMed: 30265682]
37. Darricarrère N; Pougatcheva S; Duan X; Rudicell RS; Chou TH; DiNapoli J; Ross TM; Alefantis T; Vogel TU; Kleanthous H; Wei CJ; Nabel GJ, Development of a Pan-H1 Influenza Vaccine. J Virol 2018, 92 (22), e01349–18. [PubMed: 30185594]
38. Sautto GA; Kirchenbaum GA; Abreu RB; Ecker JW; Pierce SR; Kleanthous H; Ross TM, A Computationally Optimized Broadly Reactive Antigen Subtype-Specific Influenza Vaccine Strategy Elicits Unique Potent Broadly Neutralizing Antibodies against Hemagglutinin. J Immunol 2020, 204 (2), 375–385. [PubMed: 31811019]
39. Liang K; Ricco R; Doherty CM; Styles MJ; Bell S; Kirby N; Mudie S; Haylock D; Hill AJ; Doonan CJ, Biomimetic Mineralization of Metal-Organic Frameworks as Protective Coatings for Biomacromolecules. Nature communications 2015, 6 (1), 1–8.
40. Chen N; Collier MA; Gallovic MD; Collins GC; Sanchez CC; Fernandes EQ; Bachelder EM; Ainslie KM, Degradation of Acetalated Dextran Can Be Broadly Tuned Based on Cyclic Acetal Coverage and Molecular Weight. Int J Pharm 2016, 512 (1), 147–157. [PubMed: 27543351]
41. Li Z; Cao Y; Li Y; Zhao Y; Chen X, Vaccine Delivery Alerts Innate Immune Systems for More Immunogenic Vaccination. JCI Insight 2021, 6 (7).
42. Habibi N; Christau S; Ochyl LJ; Fan Z; Hassani Najafabadi A; Kuehnhammer M; Zhang M; Helgeson M; von Klitzing R; Moon JJ; Lahann J, Engineered Ovalbumin Nanoparticles for Cancer Immunotherapy. Advanced Therapeutics 2020, 3 (10), 2000100.
43. Jeanbart L; Ballester M; de Titta A; Corthésy P; Romero P; Hubbell JA; Swartz MA, Enhancing Efficacy of Anticancer Vaccines by Targeted Delivery to Tumor-Draining Lymph Nodes. Cancer Immunol Res 2014, 2 (5), 436–47. [PubMed: 24795356]
44. Kang TH; Monie A; Wu LS; Pang X; Hung CF; Wu TC, Enhancement of Protein Vaccine Potency by in Vivo Electroporation Mediated Intramuscular Injection. Vaccine 2011, 29 (5), 1082–9. [PubMed: 21130752]
45. Shirai S; Shibuya M; Kawai A; Tamiya S; Munakata L; Omata D; Suzuki R; Aoshi T; Yoshioka Y, Lipid Nanoparticles Potentiate Cpg-Oligodeoxynucleotide-Based Vaccine for Influenza Virus. Frontiers in Immunology 2020, 10. [PubMed: 32117219]
46. Wang SH; Chen J; Smith D; Cao Z; Acosta H; Fan Y; Ciotti S; Fattom A; Baker J, A Novel Combination of Intramuscular Vaccine Adjuvants, Nanoemulsion and Cpg Produces an Effective Immune Response against Influenza a Virus. Vaccine 2020, 38 (19), 3537–3544. [PubMed: 32245642]
47. Gong M; Zhou J; Yang C; Deng Y; Zhao G; Zhang Y; Wang Y; Zhou Y; Tan W; Xu H, Insect Cell-Expressed Hemagglutinin with Cpg Oligodeoxynucleotides Plus Alum as an Adjuvant Is a Potential Pandemic Influenza Vaccine Candidate. Vaccine 2012, 30 (52), 7498–7505. [PubMed: 23116697]
48. Huang M-H; Lin S-C; Hsiao C-H; Chao H-J; Yang H-R; Liao C-C; Chuang P-W; Wu H-P; Huang C-Y; Leng C-H; Liu S-J; Chen H-W; Chou A-H; Hu AY-C; Chong P, Emulsified Nanoparticles Containing Inactivated Influenza Virus and Cpg Oligodeoxynucleotides Critically Influences the Host Immune Responses in Mice. PLoS One 2010, 5 (8), e12279. [PubMed: 20808862]
49. Brazolot Millan CL; Weeratna R; Krieg AM; Siegrist CA; Davis HL, Cpg DNA Can Induce Strong Th1 Humoral and Cell-Mediated Immune Responses against Hepatitis B Surface Antigen in Young Mice. Proc Natl Acad Sci U S A 1998, 95 (26), 15553–8. [PubMed: 9861007]
50. Moore KM; Batty CJ; Stiepel RT; Genito CJ; Bachelder EM; Ainslie KM, Injectable, Ribbon-Like Microconfetti Biopolymer Platform for Vaccine Applications. ACS Appl Mater Interfaces 2020, 12 (35), 38950–38961. [PubMed: 32805875]
51. Collier MA; Junkins RD; Gallovic MD; Johnson BM; Johnson MM; Macintyre AN; Sempowski GD; Bachelder EM; Ting JP; Ainslie KM, Acetalated Dextran Microparticles for Codelivery of Sting and Tlr7/8 Agonists. Mol Pharm 2018, 15 (11), 4933–4946. [PubMed: 30281314]
52. Frey A; Di Canzio J; Zurakowski D, A Statistically Defined Endpoint Titer Determination Method for Immunoassays. J Immunol Methods 1998, 221 (1–2), 35–41. [PubMed: 9894896]

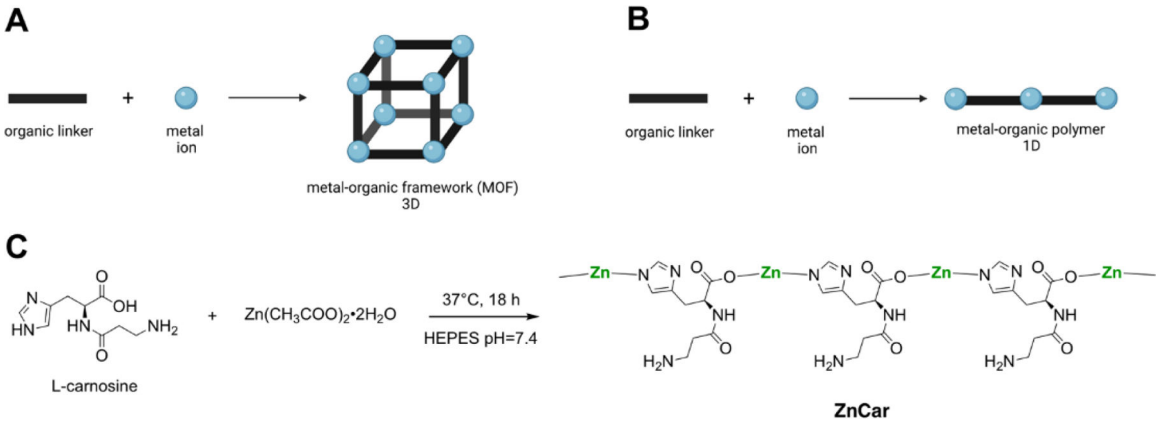

Figure 1.

(A) Schematic of 3D metal-organic framework (MOF) formation. (B) Schematic of 1D metal-organic coordination polymer formation. (C) Zinc-carnosine (ZnCar) coordination polymer formed at neutral pH in HEPES buffer.

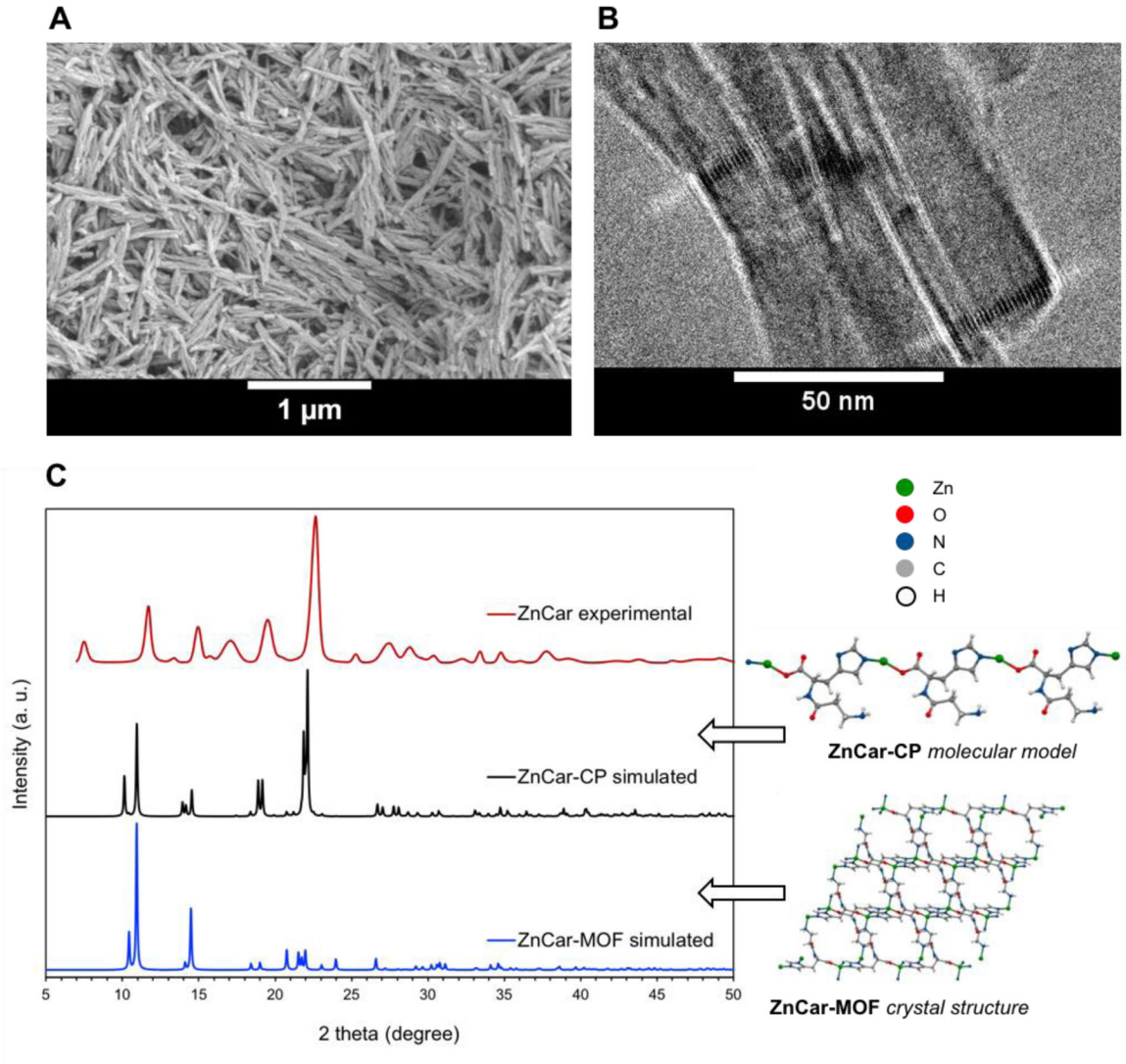

Figure 2.

(A) Scanning electron micrograph of ZnCar. (B) Cryogenic electron micrograph of ZnCar displaying lattice fringes indicative of stacks of polymeric chains. (C) PXRD pattern of ZnCar as synthesized (ZnCar experimental), compared with PXRD pattern simulated from crystal structure of ZnCar-MOF (DMF solvate) reported in literature[7] and PXRD pattern simulated from a molecular model of ZnCar coordination polymer (ZnCar-CP). ZnCar-MOF and ZnCar-CP structures are shown along the *b* crystallographic axes. Broadening of experimental spectrum relative to simulated spectrum is attributed to small size of individual crystallites composing the material as described in literature by Scherrer equation.[18]

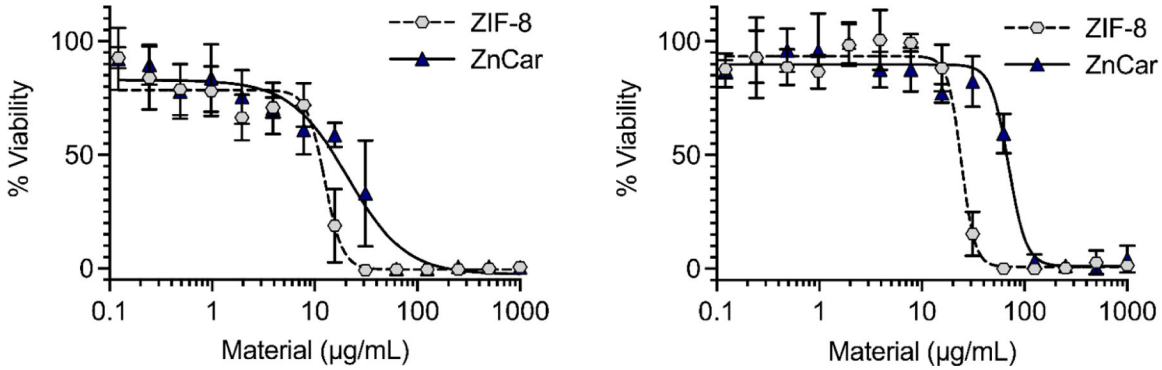

Figure 3.

In vitro biocompatibility of ZIF-8 and ZnCar measured by MTT assay. Cell viability of (A) fibroblasts (3T3) and (B) dendritic cells (DCs; DC2.4) incubated with different concentrations of ZIF-8 and ZnCar for 48 h. Data is presented as average ± standard deviation (n=6 to 12). % Viability is normalized to media only control.

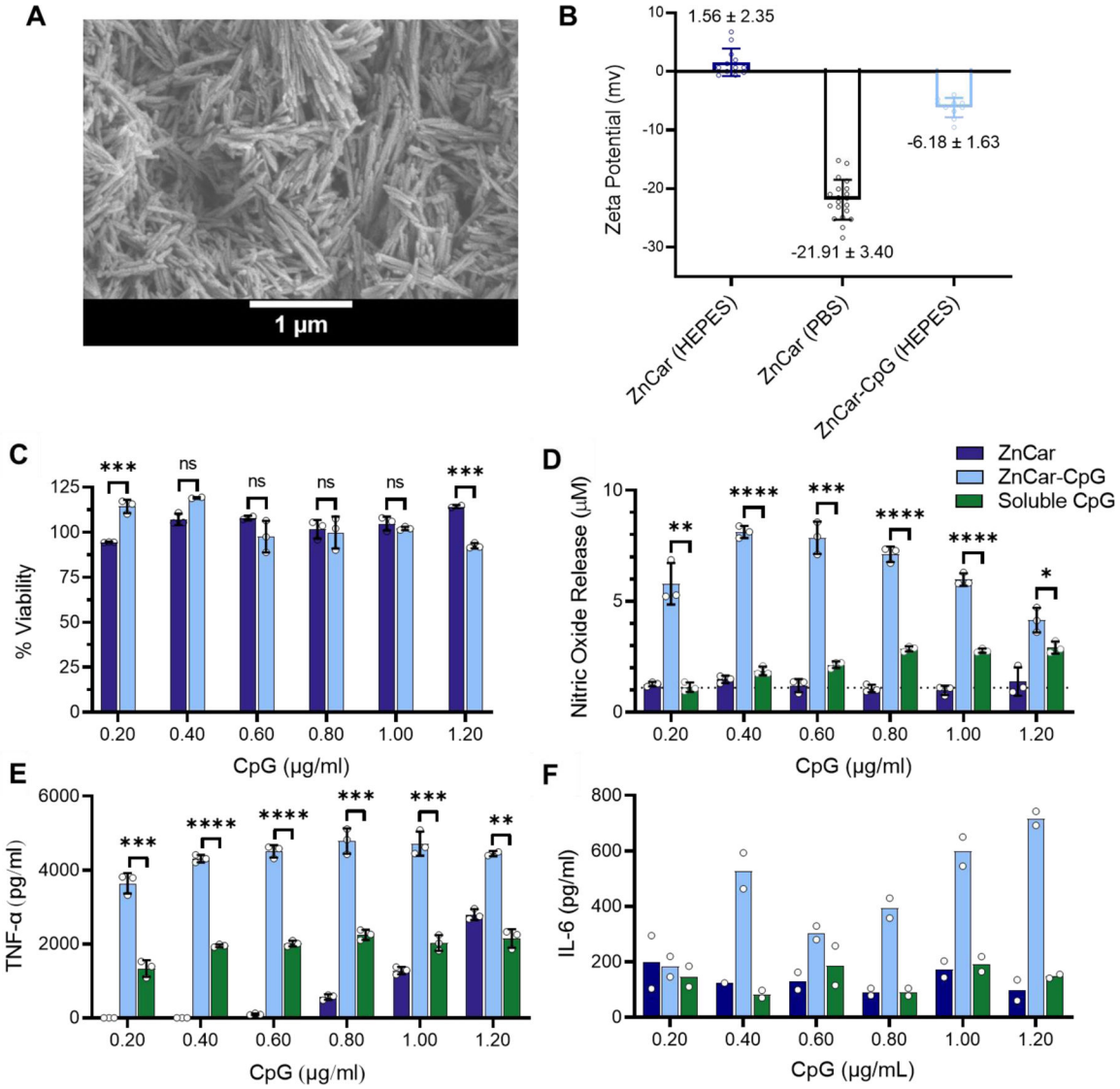

Figure 4.

(A) Scanning electron micrograph of ZnCar-CpG. (B) Zeta potential of ZnCar after incubation in HEPES buffer or PBS buffer, and ZnCar-CpG after incubation in HEPES buffer (incubation time 3 h for all samples). Zeta potentials reported as average ± standard deviation (SD). Number of data points 10–20. (C) Cell viability of macrophages incubated with different concentrations of ZnCar and ZnCar-CpG for 24 h measured by MTT assay. Empty ZnCar did not contain CpG and contained equivalent concentration of ZnCar as ZnCar-CpG material at indicated concentrations. Data is presented as average ± standard deviation (n=3). % Viability is normalized to media only control. (D) Nitric oxide (NO) released by macrophages with soluble CpG, ZnCar, and ZnCar-CpG. Data is presented as average ± standard deviation (n=3). Secretion of (E) TNF-α (F) IL-6 by macrophages incubated with indicated concentrations of soluble CpG, ZnCar-CpG, or ZnCar for 24 hr. Empty ZnCar did not contain CpG and contained equivalent concentration of ZnCar as ZnCar-CpG material at indicated concentrations. Concentration of IL-6 and TNF-α were

determined by ELISA. Data is presented as average ± standard deviation (n=3 for TNF-α and n=2 for IL-6). Unpaired t-tests were performed between ZnCar-CpG and soluble CpG at each concentration. Significance reported as * = $p \leq 0.05$, ** = $p \leq 0.01$, *** = $p \leq 0.001$, **** = $p \leq 0.0001$. ns = not statistically significant.

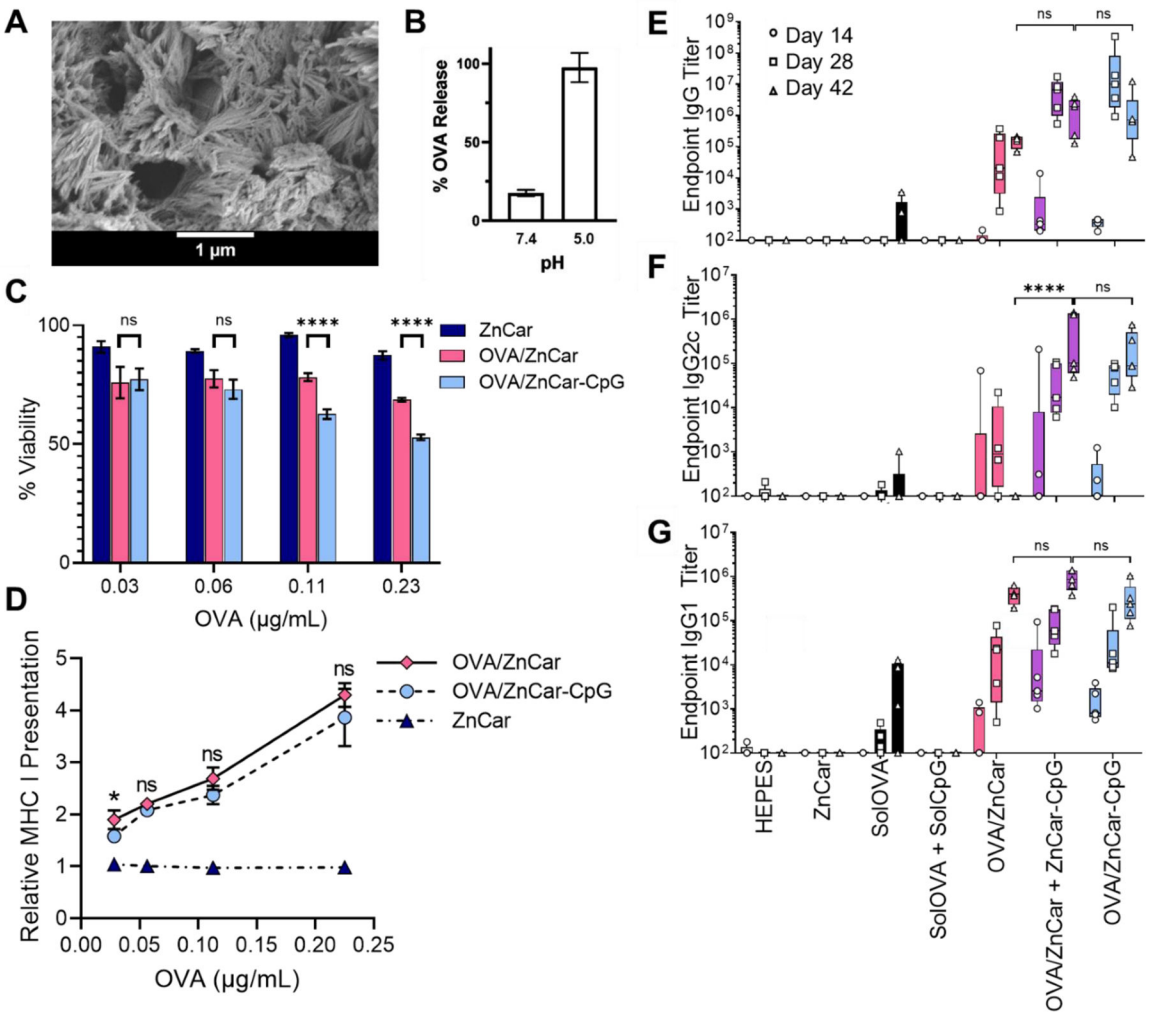

Figure 5.

(A) Scanning electron micrograph of OVA/ZnCar. (B) OVA release from OVA/ZnCar after 24 h at pH 7.4 and 5.0. (C) Cell viability of DCs (DC2.4s) incubated with different concentrations of ZnCar, OVA/ZnCar, and OVA/ZnCar-CpG for 24 h measured by MTT assay. Empty ZnCar did not contain OVA and contained equivalent concentration of ZnCar as OVA/ZnCar material at indicated concentrations. Data is presented as average ± standard deviation (n=3). % Viability is normalized to media only control. One-way ANOVA coupled with Tukey's correction for multiple comparisons was performed and significance between OVA/ZnCar and OVA/ZnCar-CpG is indicated as follows: **** = $p \leq 0.0001$. (D) Relative MHC I presentation by DCs (DC2.4s) for ZnCar, OVA/ZnCar, and OVA/ZnCar-CpG. Data is presented as the average fold change vs. soluble protein ± standard deviation (n=3). One-way ANOVA coupled with Tukey's correction for multiple comparisons was performed and significance between the OVA/ZnCar and OVA/ZnCar-CpG groups is represented as * = $p \leq 0.05$. OVA-specific (E) total IgG, (F) IgG2c, and (G) IgG1 antibody titers of mice (n=5 per group) vaccinated intramuscularly on days 0 and 21 with indicated experimental groups. Groups receiving OVA received 10 μg per mouse per dose. Groups receiving CpG received 10 μg per mouse per dose. Data is presented as average ± standard deviation. One-way

ANOVA coupled with Tukey's correction for multiple comparisons was performed for day 42 titers and significance is indicated as follows: **** = $p \leq 0.0001$. ns = not statistically significant.

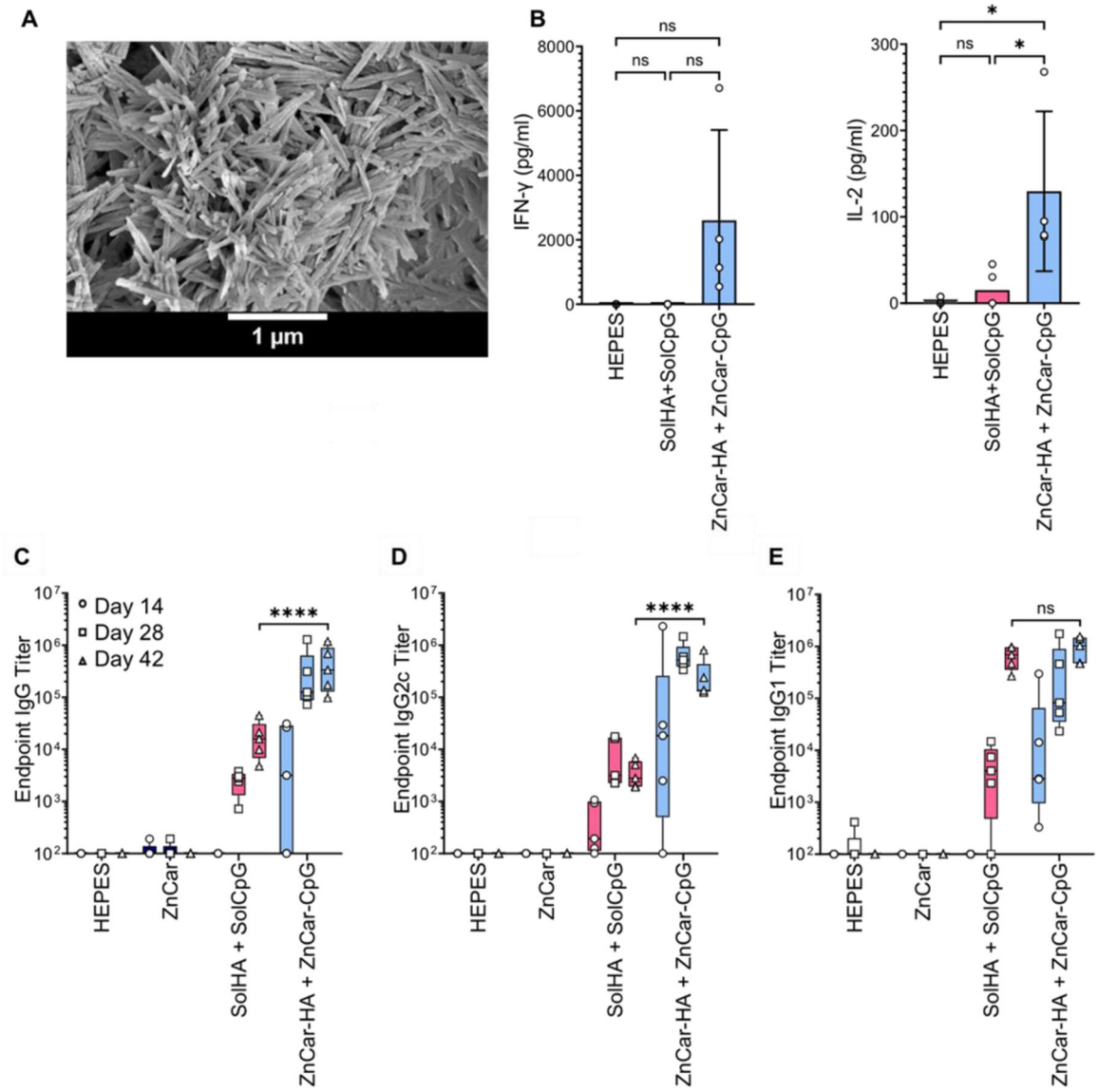

Figure 6.

(A) Scanning electron micrograph of ZnCar-HA. (B) Secretion of IL-6 and TNF-α incubated with indicated concentrations of HEPES, solHA + solCpG, and ZnCar-CpG + ZnCar-HA, where "sol" stands for soluble. Concentration of IL-6 and TNF-α were determined by ELISA. Data is presented as average ± standard deviation (n=4 to 5) One-way ANOVA coupled with Tukey's correction for multiple comparisons was performed and significance is indicated as follows: * = $p \leq 0.05$. Serum HA-specific (C) total IgG, (D) IgG2c, and (E) IgG1 antibody titers of mice (n=5 per group) vaccinated intramuscularly on days 0 and 21 with indicated experimental groups. Groups receiving HA received 10 µg per mouse per dose (HA type: COBRA P1). Groups receiving CpG received 10 µg per mouse per dose. Data is presented as average ± standard deviation. One-way ANOVA coupled with Tukey's correction for multiple comparisons was performed for day 42 titers and significance is indicated as follows: **** = $p \leq 0.0001$. ns = not statistically significant.

Table 1.

50% inhibitory concentration (IC_{50}) of ZIF-8 and ZnCar. Average ± standard deviation (n=6–12).

	50% Inhibitory Concentration (IC_{50}; μg/mL)			
	ZIF-8		**ZnCar**	
Time (h)	**24**	**48**	**24**	**48**
Fibroblasts	19.3 ± 0.6	12.5 ± 0.6	24.6 ± 1.0	20.9 ± 2.1
Dendritic Cells	25.0 ± 1.0	24.2 ± 1.3	48.6 ± 2.2	69.8 ± 4.2